Poster Presentation International Conference on Clouds and Precipitation
July 7-11, 2008, Cancun, Mexico

ROLE OF GRAVITY WAVES IN DETERMINING CIRRUS CLOUD PROPERTIES

David O'C. Starr[1], Tamara Singleton[2] and Ruei-Fong Lin[3,1]

Laboratory for Atmospheres
NASA Goddard Space Flight Center
Greenbelt, Maryland

[2]*Department of Mathematics*
University of Maryland, College Park

[3]*Goddard Earth Sciences and Technology Center*
University of Maryland, Baltimore County

Abstract

Cirrus clouds are important in the Earth's radiation budget. They typically exhibit variable physical properties within a given cloud system and from system to system. Ambient vertical motion is a key factor in determining the cloud properties in most cases. The obvious exception is convectively generated cirrus (anvils), but even in this case, the subsequent cloud evolution is strongly influenced by the ambient vertical motion field. It is well know that gravity waves are ubiquitous in the atmosphere and occur over a wide range of scales and amplitudes. Moreover, researchers have found that inclusion of statistical account of gravity wave effects can markedly improve the realism of simulations of persisting large-scale cirrus cloud features. Here, we use a 1-dimensional (z) cirrus cloud model, to systematically examine the effects of gravity waves on cirrus cloud properties. The model includes a detailed representation of cloud microphysical processes (bin microphysics and aerosols) and is run at relatively fine vertical resolution so as to adequately resolve nucleation events, and over an extended time span so as to incorporate the passage of multiple gravity waves. The prescribed gravity waves "propagate" at 15 m s^{-1}, with wavelengths from 5 to 100 km, amplitudes range up to 1 m s^{-1}. Despite the fact that the net gravity wave vertical motion forcing is zero, it will be shown that the bulk cloud properties, e.g., vertically-integrated ice water path, can differ quite significantly from simulations without gravity waves and that the effects do depend on the wave characteristics. We conclude that account of gravity wave effects is important if large-scale models are to generate realistic cirrus cloud property climatology (statistics).

ESTIMATION OF THE DEPOSTION RATE IN CIRRUS USING RAMAN LIDAR AND CLOUD RADAR

Ruei-Fong Lin[1,2], Jennifer M. Comstock[3], David O'C. Starr[2]

1 - Goddard Earth Sciences and Technology Center, University of Maryland, Baltimore County, Baltimore, Maryland, USA
2 - Laboratory for Atmospheres, NASA Goddard Space Flight Center, Greenbelt, Maryland, USA
3 - Pacific Northwest National Laboratory, Richland, Washington, USA

1. INTRODUCTION

The deposition rate, $\dot{\chi}$, (in units of mass of condensate per mass of air per unit time) is an essential component in cirrus evolution. If the deposition rate is known, we could explain the evolution of the observed moisture field in a more quantitative fashion. The goal of this research is to present a new method for estimating the deposition rate using ground-based remote sensing measurements.

2. MEASUREMENTS

We use measurements of the extinction coefficient, $b_{ext,L}$, from a Raman lidar (RL) and the equivalent radar reflectivity factor, Z_e, from a 35 GHz Millimeter-wave Cloud Radar (MMCR) to derive $\dot{\chi}$. Both instruments are located at the ARM Climate Research Facility (ACRF) Southern Great Plains (SGP) site. The different but complimentary operating wavelengths (Donovan and van Lammeren, 2001) make the retrieval of $\dot{\chi}$ possible. Details for both the ARM RL and MMCR can be found at http://www.arm.gov.

The parameter $b_{ext,L}$ is computed from the ARM RL nitrogen channel using a procedure described in Ansmann et al. (1992). The water vapor mixing ratio q_v is computed using the ratio of the lidar signals at 408-nm (water vapor scattering) and at 387-nm (nitrogen scattering). Temperature profiles are interpolated between four times a day radiosonde profiles.

3. METHOD

In this study, we consider columns and bullet rosettes because we are mostly interested in the upper tropospheric cirrus formed in situ.

The modified Gamma function has been widely used to describe the size distribution of ice particles in cirrus clouds, i.e., $N(D)dD = \frac{N_t}{\Gamma(\nu)}(\frac{D}{D_*})^{\nu-1}\exp(-\frac{D}{D_*})\frac{dD}{D_*}$, where D is the particle maximum dimension, N_t is the number of particles per unit volume, ν is a parameter controlling the width of the distribution and D_* is a characteristic length. Note that $D_*(\nu-1)$ is the modal length. An advantage of this practice is that a simple formula results for the moments. Thus, if a particle property can be formulated or approximated by a power-law function (i.e. $x = \alpha D^{\beta}$), its integrated property over the entire size distribution can be obtained easily.

The extinction coefficient $b_{ext,L}$ is a moment of the particle size distribution (PSD), $b_{ext,L} \approx 2\int A(D)N(D)dD$, where A is the particle cross section and $N(D)$ is the size distribution function. The power-law relationship between A and D has been observed from various studies and is summarized in Heymsfield and Miloshevich (2003).

Analogously, Z_e is also a moment of the PSD, $Z_e = \frac{\lambda^4}{\pi^5 |k_w|^2} \int \sigma_R(D) N(D) dD$, where σ_R is the backscatter cross section, λ is the wavelength, and $|k_w|^2$ is the dielectric constant for water particles. The power-law relationship between σ_R and D has been given in Aydin and Walsh (1999).

The power law relationship is suitable to describe the relationship between the ice crystal growth and its maximum dimension because the approximation error is within 10% when using 2 or 3 segments to capture the full parameter range. In this work, the capacitances of bullet rosettes and columns are formulated according to Chiruta and Wang (2003) and the spheroid approximation, respectively. The actual value of the deposition coefficient, β_i, is still a debatable question. Thus, we use a sensitivity test approach to examine its effect. It is set to 0.006 (slow growth, e.g., Magee et al., 2006), 0.1, or 1 (fast growth) in the calculations.

The flowchart of the procedure is briefly illustrated in Figure 1. First, R, the ratio of $b_{ext,L}$ and Z_e times a constant, is used to obtain D_*, which is then used to acquire N_t. The parameter ν is set to 2 after tests confirm a less than 10% sensitivity to the parameter by varying its value between 1 and 3. Note that in the procedure, the incomplete gamma function is used to account for segments of power-law relationship. A similar approach has been adopted to retrieve ice water content (IWC) and mass median size using the zeroth and first moments of the Doppler spectrum from a millimeter-wavelength Doppler radar (Mace et al., 2002).

4. RESULTS

A cirrus observed on 7 December 1999 is examined in this study. A modeling study of the same cloud system is reported in Comstock et al. (2008). The RL and MMCR measurements are plotted in Figure 2. Note that the uncertainty for the RL measured q_v increases from ~10% at z = 8.5 km to ~30% near the cloud top. Roughly 25% of cloudy pixels in the upper cirrus are highly ice supersaturated (RHI>120%).

Spotty high extinction ($b_{ext,L}$) regions are located near the cloud top. From our calculations, these bright spots contain many small particles (Figure 3). Nevertheless, 80% the cloudy pixels contain N_t between 5 and 500 L^{-1} where only 10% of the cloudy pixels contain N_t greater than 500 L^{-1}.

Also shown in Figure 3 is a decreasing trend of D_* with respect to height, indicating the importance of sedimentation-growth in this cloud. 90% the cloudy pixels contains PSDs of D_* less than 100 micron.

$\dot{\chi}$ in Figure 3 is calculated assuming column particles and β_i =1, which is the fastest growth scenario. The results indicate that, if those assumptions on the particle shape and the deposition coefficient are adequate, particles are uptaking water vapor very efficiently in those high ice supersaturation regions. However, this seems to directly contradict the frequent (25%) and non-spotty occurrence of high ice supersaturation in this cloud. Does this contradiction imply that β_i should be smaller than 1? It is yet too premature to make such a conclusion. More studies are needed to understand this issue.

One naturally wonders whether the significance of latent heat release in the cirrus evolution might change with β_i. From Figure 3, persistent high positive deposition rate occurs in the upper cloud between 0300 and 0400 UTC. The hourly averaged latent heating rate profiles computed from six scenarios for this period of time are compared in Figure 4. As the figure indicates, the differences are enormous. Latent heat release in the fast growth scenario would contribute significantly to buoyancy production and local circulation

whereas it plays a minor role in the cloud dynamics in the slow growth scenario.

The last panel in Figure 3 shows that a moderate (as compared to the local moisture tendency) magnitude of sublimation takes place near the cloud base. Does particle sedimentation and local sublimation result in the downward development of the cloud observed by the ground-based instruments? To answer this question, we need to examine the local q_v tendency first. Most of the pixels below z = 8.2 km has a random error less than 10%. According to our estimate, the local tendency calculated from two consecutive pixels in time has an error less than 20% when their difference is greater than 20%. We've found the uncertainty in the measured q_v does not hamper our analysis because this cloud base experiences a fast moistening that is within the measurement limit. According to our calculations, even the fastest growth scenario is not able to explain the drastic moistening near the cloud base. The moistening should have been a result of sub-grid (relative to the large-scale data derived from the constrained variational analysis) q_v forcing, i.e., likely the unresolved horizontal advection.

5. SUMMARY

A new method that estimates the deposition rate using data collected from Raman lidar and the millimeter wave cloud radar is developed to provide a more quantitative explanation of the observed water vapor evolution in the upper troposphere. In the selected case, regions with largest ice supersaturation ratios and deposition rates located were found near cloud top where plenty of small particles are present. This suggests a nucleation process in action. Moreover, a small particle regime is particularly sensitivie to specification of the deposition coefficient in terms of deposition rate and latent heat release. This implies that the cirrus dynamics and its evolution time scale may be closely linked to the deposition coefficient. Therefore, more studies to reduce the uncertainties in the deposition coefficient are warranted.

6. BIBLIOGRAPHY

Aydin, K., and T. M. Walsh, Millimeter wave scattering from spatial and planar bullet rosettes. IEEE Transactions on Geoscience and Remote Sensing, 37, 1138-1150, 1999.

Ansmann, A. U., Wandinger, M. Riebesell, C. Weitkamp, and W. Michaelis, Independent measurement of extinction and backscatter profiles in cirrus clouds by using a combined Raman elastic-backscatter lidar, App. Opt., 31, 7113-7131, 1992.

Chiruta, M. and P. K. Wang, The capacitance of rosette ice crystals. *J. Atmos. Sci., 60,* 836-846, 2003.

Comstock, J. M., R.-F. Lin, D. O'C. Starr, Understanding ice supersaturation, particle growth, and number concentration in cirrus clouds. *The 15th International Conference on Clouds and Precipitation,* Cancun, Mexico, July 7-11, 2008.

Donovan, D. P., and A. C. A. P. van Lammeren: Cloud effective particle size and water content profile retrievals using combined lidar and radar observations. I. Theory and examples. *J. Geophys. Res.,* 106 (D21), 27 425- 27 448, 2001.

Heymsfield, A. J., and L. M. Miloshevich, Parameterization for the cross-sectional area and extinction of cirrus and stratiform ice cloud particles. *J. Atmos. Sci., 60,* 936-956, 2003.

Mace, G. G., A. J. Heymsfield, M. R. Poellot, On retrieving the microphysical properties of cirrus clouds using the moments of the millimeter-wavelength Doppler spectrum. *J. Geophys. Res., 107,* doi:10.1029/2001JD001308, 2002.

Magee, N. A. M. Moyle, and D. Lamb, Experimental determination of the deposition coefficient of small cirrus-like ice crystals near -50°C. *Geophys. Res.*

Lett., *33*, L17813, doi:10.1029/2006GL026665, 2006.

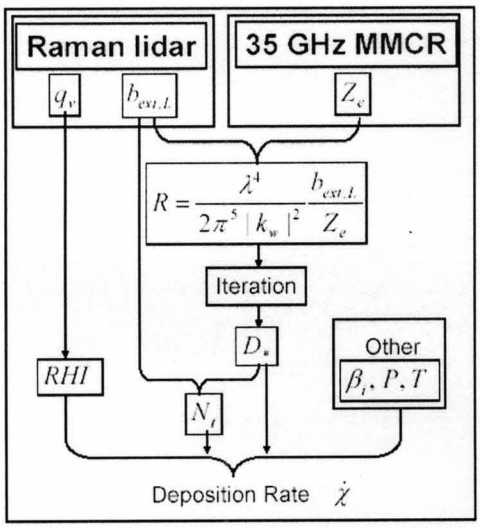

Figure 1. Flowchart.

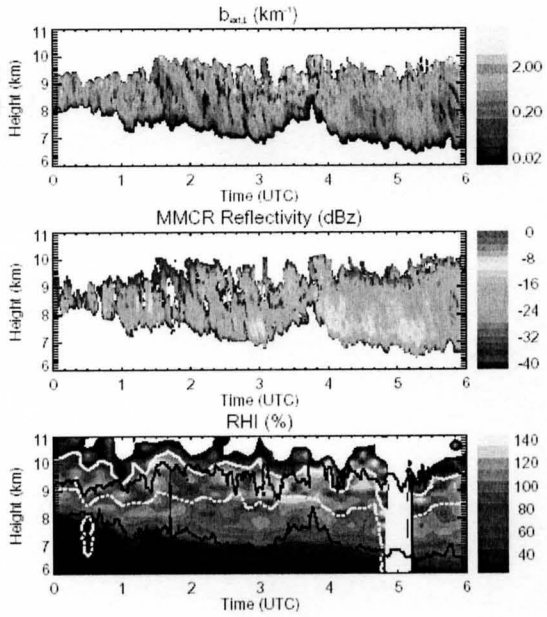

Figure 2. Height-time sections of the RL extinction coefficient, radar reflectivity, and RHI. In the last panel, the black, white solid, and white dash-dotted curves indicate the cloud boundaries, the 30% error contour, and the 10% error contour, respectively.

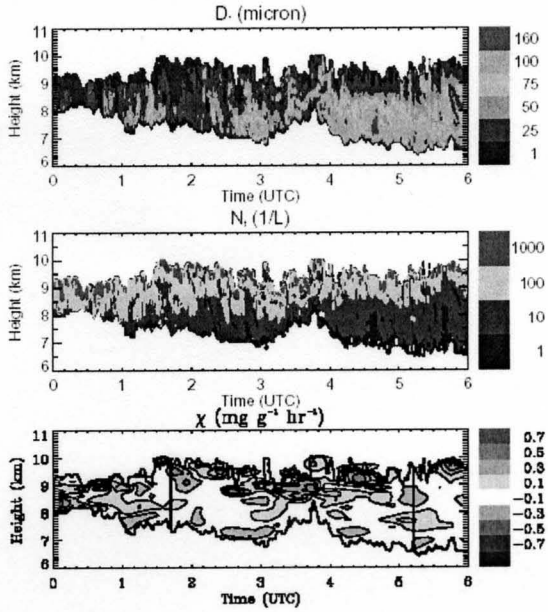

Figure 3. Height-time sections of the derived D_*, N_t, and $\dot{\chi}$. In this calculation, ν =2, β_i =1, particles are columnar.

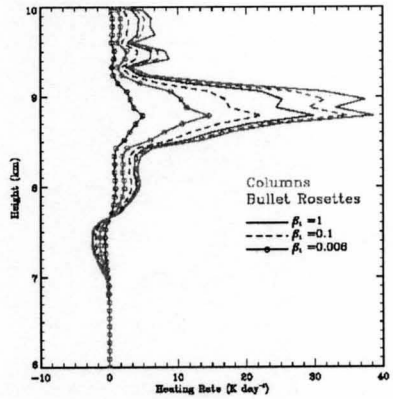

Figure 4. Heating rates due to latent heat release.